#### **ORIGINAL ARTICLE**



# Data-driven optimisation of process parameters for reducing developed surface area ratio in laser powder bed fusion

Yuchu Qin<sup>1</sup> · Peizhi Shi<sup>2</sup> · Shan Lou<sup>1</sup> · Tian Long See<sup>3</sup> · Mikdam Jamal<sup>3</sup> · Wenhan Zeng<sup>1</sup> · Liam Blunt<sup>1</sup> · Paul J. Scott<sup>1</sup> · Xiangqian Jiang<sup>1</sup>

Received: 6 November 2024 / Accepted: 8 January 2025 / Published online: 25 January 2025 © The Author(s) 2025

#### **Abstract**

Optimising process parameters is a key category of approaches to improve the surface quality of laser powder bed fusion parts. So far, many optimisation methods have been presented, which provide effective ideas and approaches for improving surface quality. However, these methods all focus on the improvement of  $R_a$ ,  $S_a$ ,  $R_{sk}$ , or  $R_{\Delta a}$ . These parameters are sufficient for most applications. They are however not suitable for applications where functional performance is linked with surface area. To quantify the quality of surfaces for these applications, the developed surface area ratio  $(S_{dr})$  is a more appropriate parameter as it can be used to quantitatively express the exposed functional surface area. In this paper, a data-driven method for optimising five process parameters, namely layer thickness, laser power, hatch spacing, point distance, and exposure time, to reduce the developed surface area ratio of laser powder bed fusion parts is proposed. Firstly, experiments are designed, and actual build and measurement experiments are conducted to acquire a fixed amount of data. A Bayesian ridge regression model for predicting a developed surface area ratio from the five process parameters is then trained and tested and compared with several other machine learning models using the acquired data. After that, optimisation of the five process parameters to reduce developed surface area ratio is carried out using the genetic algorithm, in which the objective function values (developed surface area ratios) are predicted using the established Bayesian ridge regression model. Finally, an additional actual build and measurement experiment is conducted to validate the optimisation. The testing results show that the Bayesian ridge regression model can obtain an average R<sup>2</sup> score of 0.77 and an average mean absolute error of 8.48 on the testing dataset. The validation results suggest that the developed surface area ratios generated by the optimisation are relatively small, and on average, they are 52.11% smaller than the developed surface area ratio under the process parameters recommended by the used laser powder bed fusion system.

 $\textbf{Keywords} \ \ Process \ parameter \ optimisation \cdot Surface \ quality \cdot Surface \ development \ ratio \cdot Laser \ powder \ bed \ fusion \cdot Machine \ learning \cdot Optimisation \ algorithm$ 

#### List of acronvms

LI	st of acrof	іупіз	FS	Feature selection
AM		Additive manufacturing	FT	Feature transformation
В	RR	Bayesian ridge regression	GA	Genetic algorithm
	OE	Design of experiment	GB	Gradient boosting
	DT	Decision tree	HS	Hatch spacing
	ET	Exposure time	LP	Laser power
_			LPBF	Laser powder bed fusion
⊠ Shan Lou		on ul	LR	Lasso regression
	s.lou@hud	.ac.uk	LT	Layer thickness
1	EPSRC Fu	ture Advanced Metrology Hub for Sustainable	MAE	Mean absolute error
		ring, University of Huddersfield, Huddersfield	PD	Point distance
	HD1 3DH,	UK	PP	Process parameter
School, Uni  The Manufa		Decision Research, Leeds University Business	RF	Random forest
		iversity of Leeds, Leeds LS2 9JT, UK	SS	Scanning speed
		acturing Technology Centre (MTC), Ansty Park, CV7 9JU, UK	SVR	Support vector regression



#### 1 Introduction

Laser powder bed fusion (LPBF) is an additive manufacturing (AM) technique that uses a high power-density laser beam to selectively melt and fuse metallic powders together to create three-dimensional parts with complex geometries. This technique allows the manufacture of high-value products with clear technical and economic benefits and is regarded as the key metal AM technology for producing functional components in industry [1–5].

Despite the fundamental advantages enabled by LPBF, there are still several challenges hindering its wider application [6]. One of the challenges lies in poor surface quality, associated with excessive surface roughness. It is well known that surface quality is one of the most important part quality indicators in terms of tolerance and fits. An LPBF part with poor surface quality could be difficult to assemble and therefore requires additional machining operations. Further, rough surfaces have deleterious effects on the fatigue performance of a part [7, 8].

In recent years, many researchers explored approaches to improve the surface quality of LPBF parts [9]. An important category of approaches is by optimising build orientation and layer thickness (LT) [10–12]. Campbell et al. [13] presented an analytical model that aims to reduce surface roughness  $(R_a)$  via optimising build orientation and LT. Ahn et al. [14] established an empirical model that is based on the measured roughness  $(R_a)$  data under a set of build orientations and numerical interpolation. To leverage both the analytical and empirical models, Strano et al. [15], Brika et al. [16], and Boschetto et al. [17] introduced several hybrid approaches. Strano et al. [15] modelled the surface roughness  $(R_a)$  of stainless steel (316L) parts via build orientation, LT, and particle presence and adopted the measured roughness data to calibrate the analytical model. Brika et al. [16] formulated surface roughness  $(R_a)$  of titanium (Ti6Al4V) parts as a linear function with respect to build orientation, whose coefficients were determined by the measured roughness data under a set of build orientations and a constant LT. Boschetto et al. [17] modelled the surface roughness  $(R_a)$  of aluminum (AlSi10Mg) parts based on build orientation, LT, and defects of the powder used and also used the measured roughness data to calibrate the analytical model.

Another important category of approaches to improve the surface quality of LPBF parts is by optimising some critical process parameters (PPs). Alrbaey et al. [18] investigated the effect of re-melting parameters on the surface roughness ( $R_a$ ) of LPBF parts. Twenty-seven stainless steel (316L) samples with varying build orientations were built, and laser re-melting was performed on these samples. The surface roughness was improved through optimising laser power (LP), scanning speed (SS), and hatch spacing (HS) in a design of experiment (DOE) framework. Chen et al. [19]

conducted a set of actual build experiments to study the variance of surface roughness  $(R_a, R_{sk}, \text{ and } R_{\Delta a})$  with respect to powder size distribution, process by-product generation, and powder packing fraction. Forty-five titanium (Ti6Al4V) parts were built in the experiments. A rational DOE was applied to optimise the LP, SS, and contour offset to enhance the quality of inclined surfaces. Elsayed et al. [20] investigated the influence of LP, SS, and HS on the porosity level, surface roughness  $(R_a)$ , elastic modulus, and compressive strength of LPBF parts. Seventeen titanium (Ti6Al4V) samples were built, and response surface methodology and analysis of variance were adopted to optimise the three PPs. Li et al. [21] experimentally studied the relationships between LP, SS, and HS and the surface roughness  $(R_a)$  of LPBF parts. Twenty titanium (Ti6Al4V) samples were built in the experiments. Response surface methodology was applied to optimise the three PPs with an objective of reducing the roughness of top and side surfaces. Majeed et al. [22] conducted a set of actual build experiments to investigate the influence of LP, SS, HS, and overlap rate on the roughness  $(R_a)$  of the front and side surfaces of LPBF parts. Eighty-one aluminum (AlSi10Mg) parts were built in the experiments. Analysis of variance was applied to obtain the best level of LP. Regression analysis was performed to optimise the SS, HS, and overlap rate for minimising the surface roughness. Deng et al. [23] studied the influence of LP, SS, and HS on the roughness  $(R_a)$  of top surfaces and relative density of LPBF parts based on 20 as-built stainless steel (316L) parts. Analysis of variance was adopted to establish quadratic response surface models for the two output responses. Multi-objective optimisation was performed to optimise the three PPs with respect to the two responses. Khorasani et al. [24] built a model to analyse the effect of LP, HS, SS, scan pattern angle, and heat treatment on the surface roughness  $(S_a)$  of LPBF parts. An artificial neural network was trained and tested using the data from 125 titanium (Ti6Al4V) samples. Experimental results showed that the ranking of the five influential PPs on the response from the highest to the lowest is heat treatment, LP, scan pattern angle, HS, and SS. Cao et al. [25] established a data-driven framework to optimise the LT, LP, and SS for enhancing the dimensional accuracy and surface quality  $(R_a)$ of LPBF parts. Using the data from 21 as-built stainless steel (316L) samples, a Gaussian process regression model was trained and tested to predict the two output responses. The whale optimisation algorithm was introduced to search the optimal combination of the three PPs, in which the fitness values corresponding to the two responses were estimated using the established Gaussian process regression model. Oyesola et al. [26] investigated the influence LP and SS on the surface hardness and roughness  $(R_a)$  of the top and side surfaces of LPBF parts based on the data from 16 as-built titanium (Ti6Al4V) samples. Response surface methodology was adopted to optimise the two PPs for enhancing



the surface hardness and quality. Lu and Shi [27] systematically investigated the effect of LT, LP, SS, and HS on the relative density and surface roughness  $(R_a)$  of LPBF parts. Thirty Inconel 718 samples were built in this investigation. Prediction models for the two output responses were established using response surface methodology and analysis of variance. Based on the prediction models, multi-objective optimisation was performed to concurrently optimise the two responses. Park et al. [28] developed a data-driven framework to relate the LT, LP, SS, and HS and the density ratio and surface roughness  $(S_a)$  of LPBF parts. A deep neural network was trained and tested based on the data from 2048 as-built titanium (Ti6Al4V) samples. The established deep neural network was used to generate the optimal combination of the four PPs that can maximise the density ratio and minimise the top surface roughness. Qin et al. [29] presented an approach for optimising the LT, LP, HS, point distance (PD), and exposure time (ET) to improve the surface quality  $(S_a)$  of LPBF parts. In this approach, DOE was adopted to generate 25 alternative combinations of the five PPs. Twentyfive stainless steel (316L) parts were built and measured to acquire the quality indicator values of the critical surfaces under each alternative combination. The optimal combination of PPs was determined using a flexible multi-attribute decision-making method.

As can be seen from the above overview, most of the existing studies focus on the improvement of  $R_a$ , while a few studies consider  $S_a$ ,  $R_{sk}$ , and  $R_{\Delta q}$ . Although these parameters are sufficient for most engineering applications, they are not suitable for the applications of surface coating, adhesion, lubricant, bio integration, and heat exchange, in which functional performance is highly linked with surface area [30, 31]. To quantify the quality of surfaces for these applications, the developed surface area ratio  $(S_{dr})$  is a more appropriate parameter as it can be used to quantitatively express exposed surface area [32–34]. However, none of the existing studies involves the improvement of the  $S_{dr}$  of LPBF parts.

In this paper, a data-driven method for optimising LT, LP, HS, PD, and ET to reduce the  $S_{dr}$  of an LPBF part is proposed to fill the research gap. This method is based on an idea of using the genetic algorithm (GA) [35] to search the optimal combination of the five PPs from infinite solution space with an objective of minimising  $S_{dr}$ , in which the objective function values are predicted using a Bayesian ridge regression (BRR) model [36] established on the basis of the data from DOE analyses [37] and a set of actual build and measurement experiments. Due to the combination of the machine learning and optimisation techniques, this high-dimensional, multimodal, and complex optimisation problem could be tackled efficiently by the method.

The remainder of the paper is organised as follows: Section 2 describes the details of the proposed method, including approaches of acquisition of experimental data, establish-

ment of the BRR model, and realisation of the optimisation of PPs. Section 3 reports the BRR model testing results and comparison and the PP optimisation results and validation. Section 4 ends the paper with a conclusion of the current work and a suggestion of future research work.

#### 2 The proposed method

In this section, the proposed data-driven method for optimising LT, LP, HS, PD, and ET to reduce the  $S_{dr}$  of an LPBF part is described and demonstrated in detail. A general flow of the method is shown in Fig. 1. The main process of the method consists of three stages: acquisition of experimental data, establishment of a prediction model, and realisation of the optimisation. In the first stage, a certain amount of experimental data is acquired via DOE analyses and actual printing and measurement experiments. Then, a BRR model for predicting the  $S_{dr}$  of an LPBF part from PPs is built based on the data in the second stage. In the last stage, optimisation of PPs to reduce  $S_{dr}$  is performed using the established BRR model and the GA.

#### 2.1 Acquisition of experimental data

#### 2.1.1 LPBF system and material

In this work, the LPBF parts were built using Renishaw AM400 and stainless steel (316L) powder supplied by Renishaw. The powder size was 15–45  $\mu$ m. The pulsed Nd:YAG laser, with a wavelength of 1070 nm, was installed in the LPBF machine. It has a maximum average laser output of 400 W. The build area has a length of 250 mm, a width of 250 mm, and a height of 300 mm. The build volume was purged using Argon gas at 22 L/min and then at 8–12 L/min during printing to maintain an oxygen concentration of less than 0.1%. The stainless steel (316L) powder supplied by Renishaw is made of iron alloyed with up to 18% of chromium mass fraction, 14% of nickel, 3% of molybdenum, 2% of manganese, and 1% of silicon, along with up to 0.1% of nitrogen mass fraction, 0.1% of oxygen, 0.045% of phosphorus, 0.03% of carbon, and 0.03% of sulphur.

#### 2.1.2 Process parameters and response

The five contour PPs, including LT, LP, HS, PD, and ET, were selected as input variables to be optimised. The reason for not selecting scanning speed is that scanning speed is defined as PD divided by ET in the Renishaw AM400 system. The range of each parameter was determined according to machine restriction and expert experience, as listed in Table 1.

The  $S_{dr}$  of the as-built parts was selected as the output response for the optimisation. According to ISO 25178-



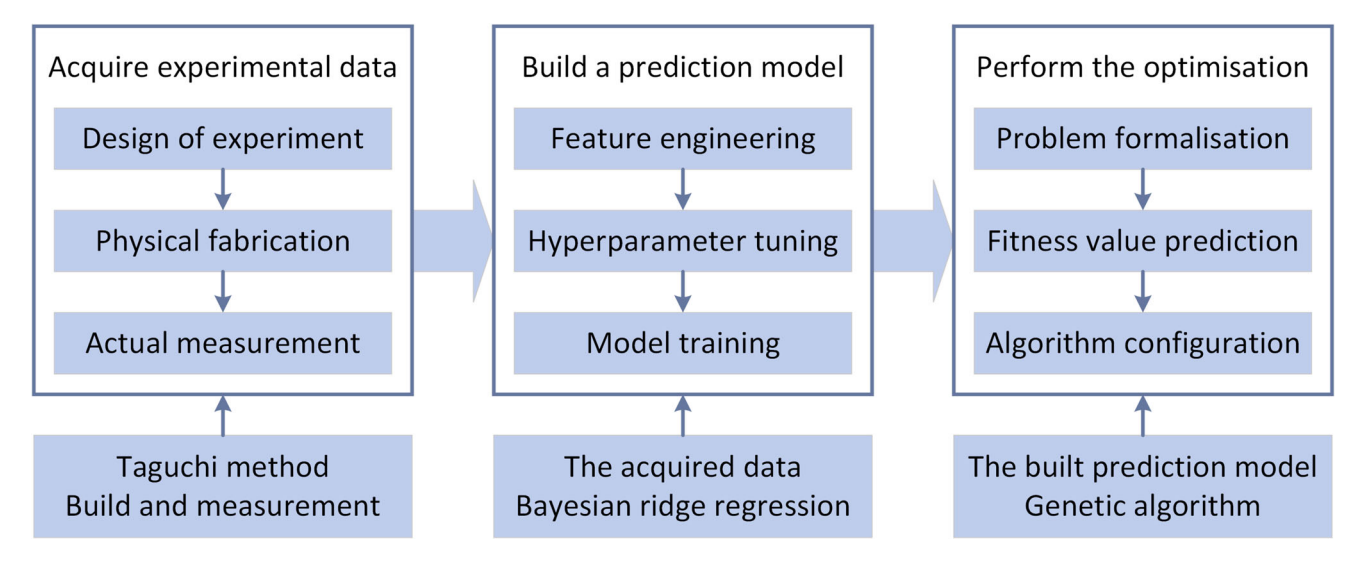


Fig. 1 General flow of the proposed data-driven method

2:2021,  $S_{dr}$  is defined as

$$S_{dr} = \frac{1}{A} \iint_{A} \left[ \sqrt{1 + \left(\frac{\partial z(x, y)}{\partial x}\right)^{2} + \left(\frac{\partial z(x, y)}{\partial y}\right)^{2}} - 1 \right] dx \, dy$$
(1)

where A is the form area. The optimisation objective is to minimise  $S_{dr}$ . It should be noted that this objective is not universal for all applications, as there are a few instances, for example in heat transfer [38] and biological tissue integration [39], where high  $S_{dr}$  is optimal. This study mainly considers the most cases. For these few applications, the only difference is to change the direction of optimisation from minimisation to maximisation of  $S_{dr}$  when configuring the optimisation algorithm.

#### 2.1.3 Printing and measurement experiments

An LPBF part as illustrated in Fig. 2 was selected as the experimental object. The study aims to investigate the reduction of the development ratio of the top surface of this part via optimisation of LT, LP, HS, PD, and ET. According to the ranges in Table 1 and practical experience, the level values of the five PPs were determined, as listed in Table 2.

Based on the level values and orthogonal array of L25, three DOE analyses were performed using Minitab 19. The results of these analyses are listed in Table 5. Using the selected LPBF system and material, 75 hexagon parts were

Table 1 Determined ranges of the PPs to be optimised

PP	LT (µm)	LP (W)	HS (μm)	PD (μm)	ET (μs)
Range	[30, 150]	[100, 200]	[25, 125]	[20, 100]	[40, 200]

Table 2 Level values of the PPs

PP	L1	L2	L3	L4	L5
LT (μm)	30	60	90	120	150
LP (W)	100	125	150	175	200
HS (µm)	25	50	75	100	125
PD (µm)	20	40	60	80	100
ET (μs)	40	80	120	160	200

built under the generated 75 combinations of PPs in Table 5, respectively.

To capture the areal topography of the top surface of each part, an Alicona G5 infinite focus variation measurement

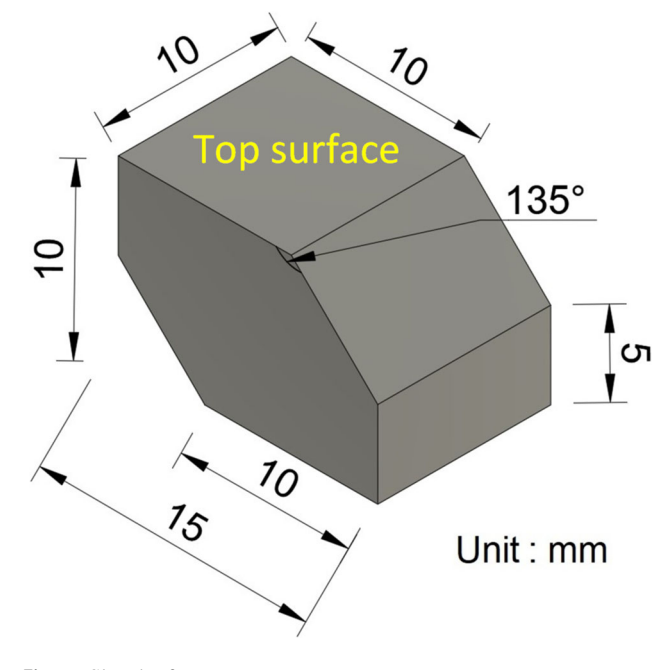


Fig. 2 Sketch of an LPBF part



system was used. The setups of the system are listed as follows: Magnification lens was  $\times$ 10; illumination type was ring light; lateral resolution was 2  $\mu$ m; vertical resolution was 1  $\mu$ m; sampling distance was 0.8780  $\mu$ m (x and y directions); measurement dimension was 8 mm  $\times$  8 mm (stitched). As an example, using the measurement system, the areal topography of the top surface of the first as-built part was captured, as depicted in Fig. 3.

The surface topographical data was analysed using DigitalSurf MountainMaps. To prevent losing surface information, only levelling was employed and no filtration procedures were carried out. The analysed data was used to generate the developed surface area ratios of the top surfaces of the 75 as-built parts. The assessed results are listed in the last column of Table 5. It is worth noting that the third as-built part was discarded since the top surface of this part is too rough to be measured with the measurement system.

#### 2.2 Establishment of a prediction model

BRR is an advanced linear model for regression problems. Bayesian principles are utilised to estimate the values of parameters in the linear model. This approach was selected as it has the potential to solve multicollinearity and overfitting issues, especially when there are only a limited number of training samples. In this approach, the linear model can be denoted as

$$y = X\beta + \epsilon, \tag{2}$$

where y refers to the predicted variable (i.e.  $S_{dr}$  value), X refers to the input variables (i.e. PP values),  $\beta$  refers to the regression coefficients, and  $\epsilon$  refers to the error term, which is assumed to follow a normal distribution. Therefore, y follows

a normal distribution with a mean of  $X\beta$  and a variance of  $\alpha^{-1}$ 

$$y \sim \mathcal{N}(X\beta, \alpha^{-1}),$$
 (3)

where  $\alpha$  refers to the precision of the error.

In the Bayesian approach, the regression coefficients  $\beta$  follow a Gaussian prior

$$\beta \sim \mathcal{N}(0, \lambda^{-1}I) \tag{4}$$

where I refers to an identity matrix, and  $\lambda$  refers to the regularising parameter. Therefore, the coefficients  $\beta$  could be determined based on the Bayes' theorem

$$p(\beta \mid y, X, \alpha, \lambda) \propto p(y \mid X, \beta, \alpha) p(\beta \mid \lambda)$$
 (5)

The precision of the error  $\alpha$  and the regularising parameter  $\lambda$  follow Gamma priors

$$\alpha \sim \mathcal{G}(\alpha_1, \alpha_2)$$
 (6)

$$\lambda \sim \mathcal{G}(\lambda_1, \lambda_2) \tag{7}$$

where  $\alpha_1$ ,  $\alpha_2$ ,  $\lambda_1$ , and  $\lambda_2$  are four hyper-parameters in this machine learning model.

Since the original dataset contains five features and the BRR model is a linear model, it may not adequately capture the potentially non-linear relationships between the process parameter values and the  $S_{dr}$  value. Therefore, a feature engineering process was carried out to achieve better predictive performance. In this approach, all polynomial combinations of the five input features with degrees less than or equal to

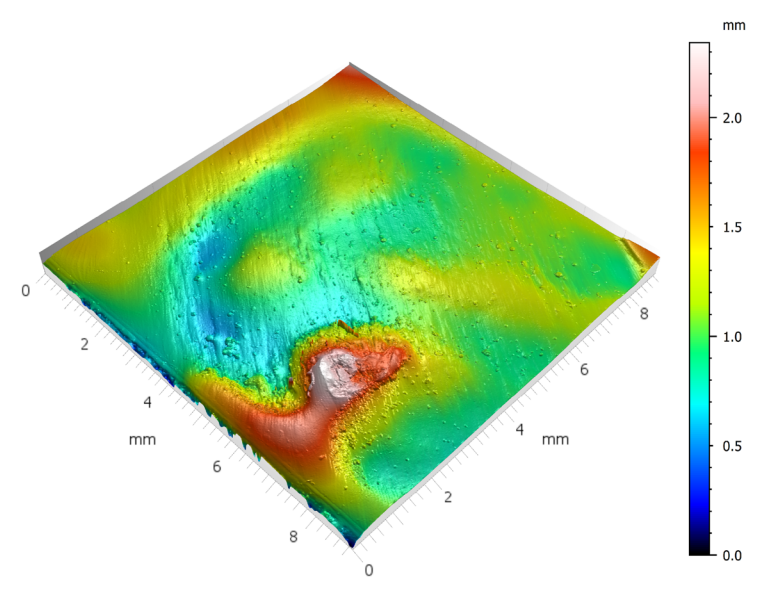


Fig. 3 Areal topography of the top surface of the 1st as-built part

**Table 3** Descriptions and assigned values of some parameters of the GA

Parameter	Description	Value
num_generations	The number of generations	50
num_parents_mating	The number of solutions to be selected as parents	4
sol_per_pop	The number of solutions within the population	80
num_genes	The number of genes in the solution	5
init_range_low	The lower value of the random range	-4
init_range_high	The upper value of the random range	5
mutation_percent_genes	The percentage of genes to mutate	10

three were generated. Then, a sequential feature selection approach was utilised to reduce the dimensionality of the data and select the most important features for prediction.

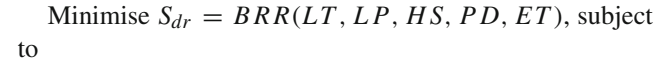
#### 2.3 Realisation of the optimisation

The GA is a meta-heuristic algorithm that mimics the natural evolution process to find the best solution. Its main working process is as follows: (1) Initialisation: A population of individuals that could be solutions is created at random. (2) Selection: A fitness function, which measures how successfully the algorithm solves a task, is used to assess each candidate. The most fit individuals are chosen to procreate. (3) Crossover: Genes are selected to produce children that combine qualities from both parents. (4) Mutation: To preserve genetic diversity, minor, random alterations are made to children's genes. (5) Replacement: The old generation is swapped out for the new one, and the cycle is repeated. The key benefits of the GA include good robustness and scalability, potential concurrency, and the ability to perform random searches unrelated to real optimisation problems [35, 40].

In this work, the GA and the established BRR model were used to optimise LT, LP, HS, PD, and ET for minimising  $S_{dr}$ . According to the determined ranges in Table 1 and machine restriction, the optimisation problem is formalised as

**Table 4** Comparison results of different machine learning models

Experiment	Model	FT	FS	$\mathbb{R}^2$	MAE
Experiment 1	BRR	<b>√</b>	<b>√</b>	0.77	8.48
Experiment 2	BRR	$\checkmark$		0.75	8.94
Experiment 3	BRR			0.70	9.78
Experiment 4	LR	$\checkmark$	$\checkmark$	0.76	8.77
Experiment 5	LR			0.69	9.83
Experiment 6	DT	$\checkmark$	$\checkmark$	0.54	12.28
Experiment 7	DT			0.48	13.18
Experiment 8	RF	$\checkmark$	$\checkmark$	0.68	10.08
Experiment 9	RF			0.68	10.22
Experiment 10	GB	$\checkmark$	$\checkmark$	0.71	9.61
Experiment 11	GB			0.70	9.92
Experiment 12	SVR	$\checkmark$	$\checkmark$	0.75	8.98
Experiment 13	SVR			0.65	10.86



 $LT \in [30, 150]$  with an increment of 30,

 $LP \in [100, 200]$  with an increment of 1,

 $HS \in [25, 125]$  with an increment of 1,

 $PD \in [20, 100]$  with an increment of 1,

 $ET \in [40, 200]$  with an increment of 10.

This problem was solved using the GA in the Python library PyGAD, in which the fitness value of a solution was predicted by the established BRR model. The configuration of the algorithm is listed in Table 3. In addition to the parameters in Table 3, all other parameters were used with their default values in PyGAD.

#### 3 Results

#### 3.1 Prediction model testing results and comparison

In this study, the BRR was compared with other regression models, including lasso regression (LR), decision tree (DT), random forest (RF), gradient boosting (GB), and support vector regression (SVR). Additionally, the benefits of feature transformation (FT) and feature selection (FS) were also evaluated. FT is capable of transforming features into another space, making it easier to identify relationships from process parameters to  $S_{dr}$ . FS helps to identify the most relevant input features, further improving performance. The sklearn library was used to establish different regression models for predicting  $S_{dr}$  from LT, LP, HS, PD, and ET. In this comparison study, 60% of the 74 data points in Table 5 were randomly selected for training, while the remaining samples were used to form a testing dataset. Grid search combined with 5-fold cross-validation was applied to the training dataset to tune the hyper-parameters of all regression models. The coefficient of determination  $(R^2)$  and mean absolute error (MAE) were used as evaluation metrics. To conduct a robust evaluation, each experiment was conducted 30 times. Each time, the original dataset was randomly split into 60% for training and 40% for testing. The averaged R<sup>2</sup> and MAE scores on the testing sets across different trials were calculated. The evaluation results are shown in Table 4.



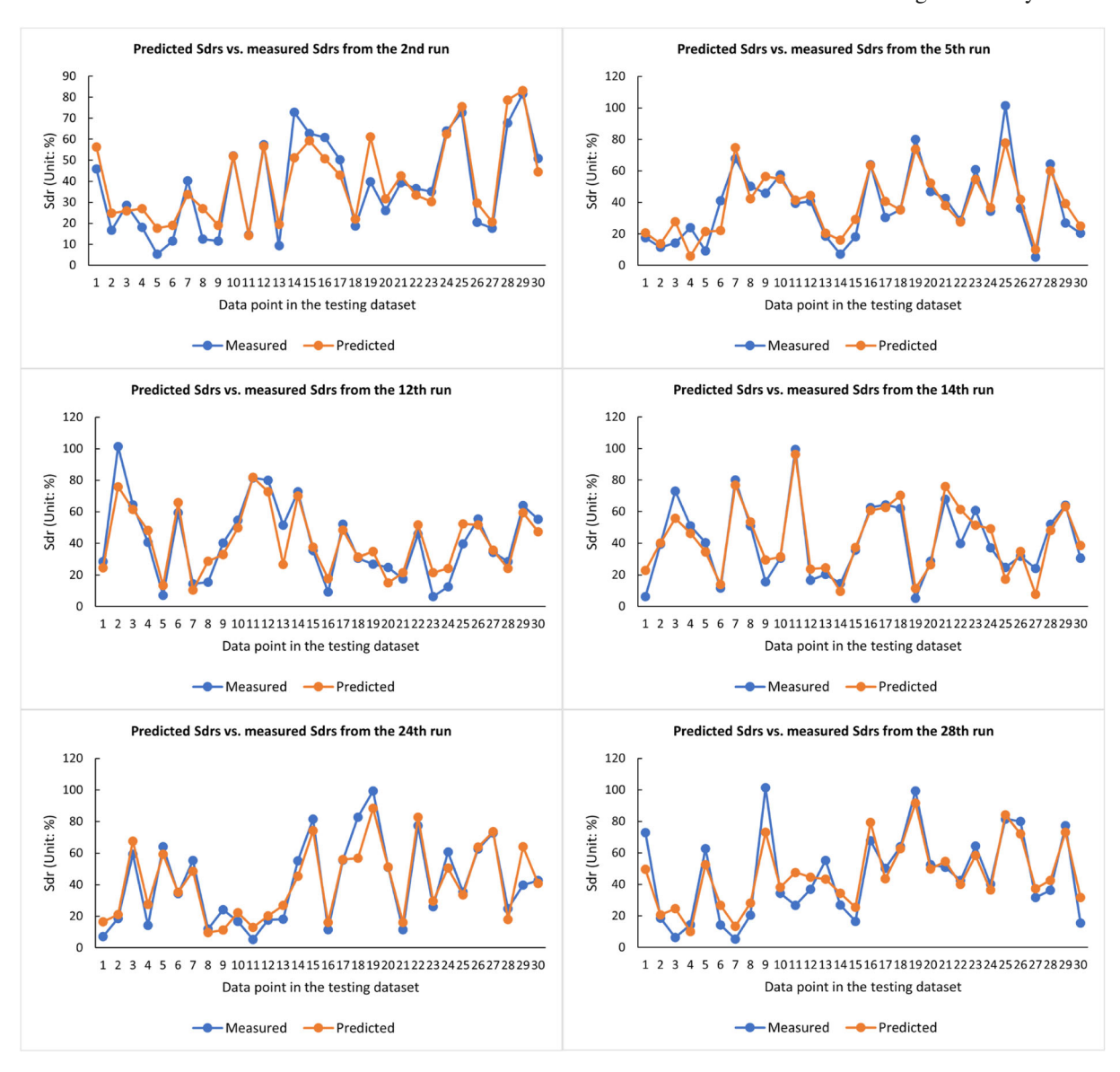
It is observed from Experiments 1 to 3 that the proposed FT and FS techniques work as expected. From Experiments 1, 2, 4, and 12, it is also evident that linear models with polynomial features and regularisation techniques produce good results. In contrast, tree-based approaches (e.g. DT, RF, GB) do not produce optimal solutions, as evident in Experiments 6 to 11. One explanation is that there might be a polynomial relationship between the PP values and the  $S_{dr}$  value. Therefore, adding these features is a good choice for this application. After FT, the dimensionality of the data increases, while the number of samples is limited. It is very likely that the machine learning models will overfit the data. The FS and regularisation techniques are beneficial in this case, as evident in Experiments 1, 4, and 12. As shown in Experiments 3, 5, 7, 9, 11, and 13, experimental settings without FT and FS produce less favourable results.

Figure 4 depicts the predicted  $S_{dr}$  versus the corresponding measured  $S_{dr}$  on the testing dataset from 6 of the 30 runs. Intuitively, the changing trend of the predicted results is generally consistent with that of the measured results for each run. This demonstrates the effectiveness of the established BRR model.

## 3.2 Process parameter optimisation results and validation

Using the configured GA, the optimal combination of PPs was generated as LT = 30  $\mu$ m, LP = 179 W, HS = 45  $\mu$ m, PD = 82  $\mu$ m, and ET = 190  $\mu$ s.

To verify the effectiveness of the proposed data-driven optimisation method, an additional validation experiment was conducted. In this experiment, the top 20 Pareto optimal combinations of PPs were first generated by the method,



**Fig. 4** Predicted  $S_{dr}$ s versus measured  $S_{dr}$ s on the testing dataset from 6 of the 30 runs

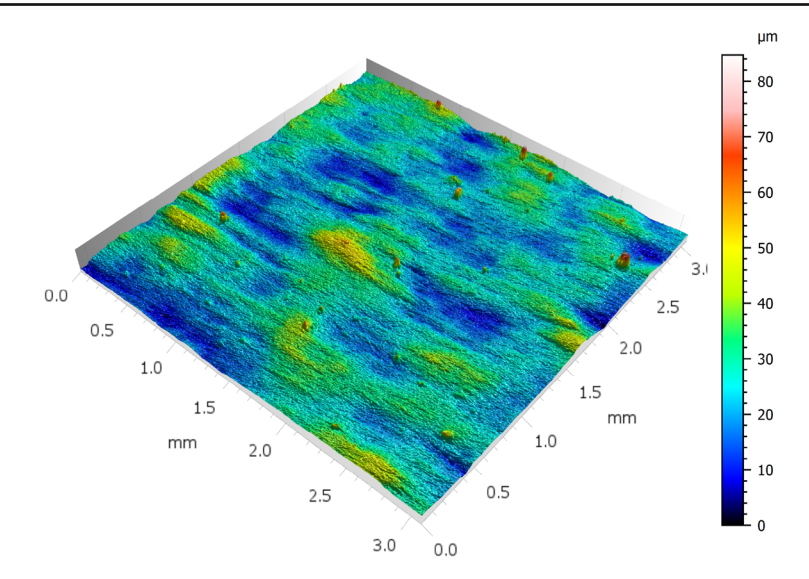


Fig. 5 Areal topography of the top surface of the 15th as-built part

as listed in Table 6. Then 20 more hexagon parts whose sketch is shown in Fig. 2 were built under the generated 20 combinations of PPs, respectively. It is worth noting that in addition to the PPs, the LPBF system and material and all other conditions remain the same as for building the 75 parts. To better show the effect of the optimisation, an additional hexagon part was built under the PPs recommended by Renishaw AM400 system, which are also listed in Table 6. Finally, the  $S_{dr}$ s of the top surfaces of the 21 as-built parts were measured using the same tools as before when measuring the top surfaces of the 75 parts. The measurement results are listed in Table 6. As an example, using the measurement system, the areal topography of the top surface of the 15th as-built part (with the smallest measured  $S_{dr}$ ) was captured, as depicted in Fig. 5. To intuitively compare the actual build and measurement results with the optimisation results, Fig. 6 depicts the changing trends of the measured  $S_{dr}$ s for the 20 parts built under the generated 20 combinations of PPs.

As can be seen from Fig. 6, all measured  $S_{dr}$ s under the top 20 Pareto optimal combinations of PPs are relatively small (between 6 and 12) compared to the measured  $S_{dr}$ s in the

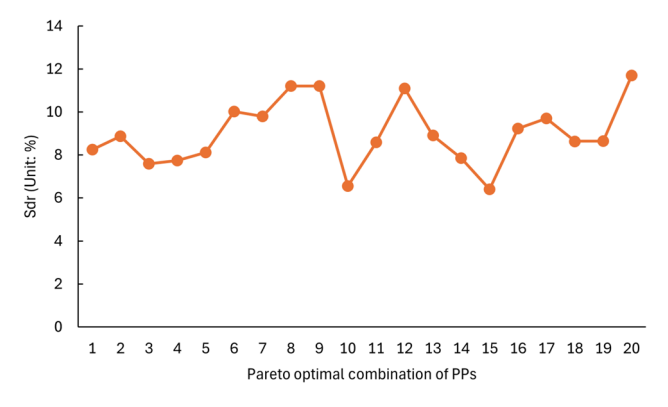


Fig. 6 Measured  $S_{dr}$ s under the top 20 optimal combinations of PPs



training dataset (Table 5). Further, all of them are obviously smaller than the  $S_{dr}$  under the combination of PPs recommended by the used Renishaw AM400 system (18.81). On average, they are 52.11% smaller than this  $S_{dr}$ . These facts demonstrate that the proposed method is effective.

#### 4 Conclusion

In this paper, a data-driven method for optimising LT, LP, HS, PD, and ET to reduce the  $S_{dr}$  of an LPBF part was presented. DOE analyses were performed, and actual build and measurement experiments were conducted to obtain a certain amount of data. Using the obtained data, a BRR model for predicting an  $S_{dr}$  from the five PPs was established and tested and compared with several other machine learning models. Optimisation of the five PPs to reduce  $S_{dr}$  was carried out using the GA and BRR model and validated through an additional actual build and measurement experiment. The testing results show that the BRR model can achieve an average R<sup>2</sup> score of 0.77 and an average MAE of 8.48 on the testing dataset. The validation results suggest that the  $S_{dr}$ s generated by the optimisation are relatively small, and on average, they are 52.11% smaller than the  $S_{dr}$  produced by LPBF system recommended PPs.

Future work will aim especially at extending the presented method through adding optimisation of build orientation. As one important class of approaches for improving the surface quality of LPBF parts is by optimisation of build orientation and LT and another important class is by optimisation of PPs, a combination of these two ways to concurrently optimise build orientation and PPs to enhance the surface quality of an LPBF part would be considered. In addition, more actual build and measurement experiments would be conducted to collect more data to build a more accurate machine learning-based prediction model. It would be interesting to include

improvement of more quality indicators of an LPBF part to the presented method to carry out data-driven multi-objective optimisation.

### **Appendix**

 Table 5
 Results of DOE analyses and measurements

No Unit	LT μm	LP W	HS μm	PD μm	$_{\mu \mathrm{s}}^{\mathrm{ET}}$	$S_{dr} \ \%$
1	30	100	25	20	40	17.64
2	60	100	50	40	80	51.46
3	90	100	75	60	120	
4	120	100	100	80	160	55.49
5	150	100	125	100	200	101.34
6	60	125	25	20	160	28.59
7	90	125	50	40	200	43.33
8	120	125	75	60	40	50.91
9	150	125	100	80	80	72.73
10	30	125	125	100	120	16.61
11	90	150	25	20	80	36.52
12	120	150	50	40	120	55.23
13	150	150	75	60	160	62.69
14	30	150	100	80	200	14.44
15	60	150	125	100	40	48.42
16	120	175	25	20	200	36.99
17	150	175	50	40	40	57.46
18	30	175	75	60	80	11.53
19	60	175	100	80	120	26.04
20	90	175	125	100	160	70.17
21	150	200	25	20	120	72.92
22	30	200	50	40	160	11.98
23	60	200	75	60	200	18.68
24	90	200	100	80	40	52.04
25	120	200	125	100	80	67.74
26	30	100	25	20	40	6.25
27	60	100	50	40	80	18.09
28	90	100	75	60	120	30.45
29	120	100	100	80	160	45.87
30	150	100	125	100	200	77.28
31	60	125	25	20	40	15.47
32	90	125	50	40	80	34.38
33	120	125	75	60	120	26.76
34	150	125	100	80	160	61.90
35	30	125	125	100	200	9.28
36	90	150	25	20	40	35.48
37	120	150	50	40	80	50.85
38	150	150	75	60	120	39.77
39	30	150	100	80	160	7.12
40	60	150	125	100	200	30.63

Table 5	continued	l				
No	LT	LP	HS	PD	ET	$S_{dr}$
Unit	μm	W	μm	μm	μs	%
41	120	175	25	20	40	40.57
42	150	175	50	40	80	45.18
43	30	175	75	60	120	5.33
44	60	175	100	80	160	14.26
45	90	175	125	100	200	55.31
46	150	200	25	20	40	60.83
47	30	200	50	40	80	5.24
48	60	200	75	60	120	12.45
49	90	200	100	80	160	39.38
50	120	200	125	100	200	59.37
51	30	100	25	60	80	24.75
52	60	100	50	60	80	28.58
53	90	100	75	60	80	36.28
54	120	100	100	60	80	63.97
55	150	100	125	60	80	99.40
56	60	125	25	60	80	41.07
57	90	125	50	60	80	40.26
58	120	125	75	60	80	60.81
59	150	125	100	60	80	80.08
60	30	125	125	60	80	26.85
61	90	150	25	60	80	35.12
62	120	150	50	60	80	50.27
63	150	150	75	60	80	64.35
64	30	150	100	60	80	16.63
65	60	150	125	60	80	46.79
66	120	175	25	60	80	42.59
67	150	175	50	60	80	52.46
68	30	175	75	60	80	11.51
69	60	175	100	60	80	31.76
70	90	175	125	60	80	82.85
71	150	200	25	60	80	39.62
72	30	200	50	60	80	24.09
73	60	200	75	60	80	20.43
74	90	200	100	60	80	54.67
75	120	200	125	60	80	81.54

**Table 6** PPs and corresponding  $S_{dr}$ s in the validation experiment

No Unit	$_{\mu \mathrm{m}}^{\mathrm{LT}}$	LP W	$_{\mu \mathrm{m}}^{\mathrm{HS}}$	$_{\mu \mathrm{m}}^{\mathrm{PD}}$	$_{\mu \mathrm{s}}^{\mathrm{ET}}$	$S_{dr}$ %
1	30	179	45	82	190	8.25
2	30	184	29	82	120	8.88
3	30	179	29	82	130	7.59
4	30	189	45	75	140	7.73
5	30	189	45	69	150	8.12
6	30	179	57	82	120	10.02
7	30	179	89	99	140	9.80



Table 6 continued								
No Unit	LT μm	LP W	HS μm	PD μm	ET μs	$S_{dr}$ %		
8	30	179	52	79	120	11.21		
9	30	177	89	99	140	11.22		
10	30	189	45	65	180	6.55		
11	30	189	45	65	170	8.60		
12	30	179	62	82	120	11.09		
13	30	179	29	71	120	8.91		
14	30	189	44	65	150	7.86		
15	30	179	29	82	70	6.40		
16	30	189	45	82	70	9.23		
17	30	179	26	65	150	9.70		
18	30	179	52	65	190	8.64		
19	30	189	45	65	130	8.64		
20	30	177	89	82	190	11.71		
R	50	110	110	20	100	18.81		

Notes: The PPs in row R were recommended by Renishaw AM400 system

**Funding** Yuchu Qin would like to acknowledge the support of the National Natural Science Foundation of China (No. 52105511). The authors are grateful to the support by the EPSRC Future Advanced Metrology Hub for Sustainable Manufacturing (Ref. EP/Z53285X/1).

**Data Availability** All related data are included in the main text and appendix of the paper.

#### **Declarations**

**Ethical approval** This paper does not contain any studies with human participants or animals performed by any of the authors.

**Conflict of interest** The authors declare no competing interests.

**Generative AI and AI-assisted technologies** The authors did not use any generative AI and AI-assisted technologies in the writing process of this paper.

Open Access This article is licensed under a Creative Commons Attribution 4.0 International License, which permits use, sharing, adaptation, distribution and reproduction in any medium or format, as long as you give appropriate credit to the original author(s) and the source, provide a link to the Creative Commons licence, and indicate if changes were made. The images or other third party material in this article are included in the article's Creative Commons licence, unless indicated otherwise in a credit line to the material. If material is not included in the article's Creative Commons licence and your intended use is not permitted by statutory regulation or exceeds the permitted use, you will need to obtain permission directly from the copyright holder. To view a copy of this licence, visit http://creativecommons.org/licenses/by/4.0/.



- Gibson I, Rosen DW, Stucker B, Khorasani M, Rosen D, Stucker B et al (2021) Additive manufacturing technologies. 3rd ed, Springer Cham
- Chua CK, Leong KF (2017) 3D printing and additive manufacturing: principles and applications. 5th ed. World Scientific Publishing
- Sing SL, Yeong WY (2020) Laser powder bed fusion for metal additive manufacturing: perspectives on recent developments. Virtual and Physical Prototyping. 15(3):359–370
- Gu D, Shi X, Poprawe R, Bourell DL, Setchi R, Zhu J (2021) Material-structure-performance integrated laser-metal additive manufacturing. Science 372(6545):eabg1487
- Bai R, Shi S, Wang J, Luo J, Pu H, Lyu W et al (2024) Investigation of printing turn angle effects on structural deformation and stress in selective laser melting. Materials & Design. 247:113347
- King WE, Anderson AT, Ferencz RM, Hodge NE, Kamath C, Khairallah SA et al (2015) Laser powder bed fusion additive manufacturing of metals; physics, computational, and materials challenges. Appl Phys Rev 2(4):041304
- Rott S, Ladewig A, Friedberger K, Casper J, Full M, Schleifenbaum JH (2020) Surface roughness in laser powder bed fusion-Interdependency of surface orientation and laser incidence. Addit Manuf 36:101437
- Snyder JC, Thole KA (2020) Understanding laser powder bed fusion surface roughness. J Manuf Sci Eng 142(7):071003
- Hashmi AW, Mali HS, Meena A (2023) A comprehensive review on surface quality improvement methods for additively manufactured parts. Rapid Prototyp J 29(3):504–557
- Qin Y, Qi Q, Shi P, Scott PJ, Jiang X (2020) Automatic generation of alternative build orientations for laser powder bed fusion based on facet clustering. Virtual Phys Prototyp 15(3):307–324
- Qin Y, Qi Q, Shi P, Scott PJ, Jiang X (2021) Automatic determination of part build orientation for laser powder bed fusion. Virtual Phys Prototyp 16(1):29–49
- Qin Y, Qi Q, Shi P, Scott PJ, Jiang X (2021) Status, issues, and future of computer-aided part orientation for additive manufacturing. Int J Adv Manuf Technol 115:1295–1328
- Campbell RI, Martorelli M, Lee HS (2002) Surface roughness visualisation for rapid prototyping models. Comput Aided Des 34(10):717–725
- Ahn D, Kim H, Lee S (2009) Surface roughness prediction using measured data and interpolation in layered manufacturing. J Mater Process Technol 209(2):664–671
- Strano G, Hao L, Everson RM, Evans KE (2013) Surface roughness analysis, modelling and prediction in selective laser melting. J Mater Process Technol 213(4):589–597
- Brika SE, Zhao YF, Brochu M, Mezzetta J (2017) Multi-objective build orientation optimization for powder bed fusion by laser. J Manuf Sci Eng 139(11):111011
- Boschetto A, Bottini L, Veniali F (2017) Roughness modeling of AlSi10Mg parts fabricated by selective laser melting. J Mater Process Technol 241:154–163
- Alrbaey K, Wimpenny D, Tosi R, Manning W, Moroz A (2014) On optimization of surface roughness of selective laser melted stainless steel parts: a statistical study. J Mater Eng Perform 23:2139–2148
- Chen Z, Wu X, Tomus D, Davies CH (2018) Surface roughness of selective laser melted Ti-6Al-4V alloy components. Addit Manuf 21:91–103
- Elsayed M, Ghazy M, Youssef Y, Essa K (2018) Optimization of SLM process parameters for Ti6Al4V medical implants. Rapid Prototyping Journal. 25(3):433–447
- Li Z, Kucukkoc I, Zhang DZ, Liu F (2018) Optimising the process parameters of selective laser melting for the fabrication of Ti6Al4V alloy. Rapid Prototyp J 24(1):150–159



- Majeed A, Ahmed A, Salam A, Sheikh MZ (2019) Surface quality improvement by parameters analysis, optimization and heat treatment of AlSi10Mg parts manufactured by SLM additive manufacturing. Int J Light Mater Manuf 2(4):288–295
- Deng Y, Mao Z, Yang N, Niu X, Lu X (2020) Collaborative optimization of density and surface roughness of 316L stainless steel in selective laser melting. Materials 13(7):1601
- Khorasani AM, Gibson I, Ghasemi A, Ghaderi A (2020) Modelling of laser powder bed fusion process and analysing the effective parameters on surface characteristics of Ti-6Al-4V. Int J Mech Sci 168:105299
- Cao L, Li J, Hu J, Liu H, Wu Y, Zhou Q (2021) Optimization of surface roughness and dimensional accuracy in LPBF additive manufacturing. Opt Laser Technol 142::107246
- Oyesola M, Mpofu K, Mathe N, Fatoba S, Hoosain S, Daniyan I (2021) Optimization of selective laser melting process parameters for surface quality performance of the fabricated Ti6Al4V. Int J Adv Manuf Technol 114:1585–1599
- Lu C, Shi J (2022) Relative density and surface roughness prediction for Inconel 718 by selective laser melting: central composite design and multi-objective optimization. Int J Adv Manuf Technol 119:3931–3949
- Park HS, Nguyen DS, Le-Hong T, Van Tran X (2022) Machine learning-based optimization of process parameters in selective laser melting for biomedical applications. J Intell Manuf 33(6):1843– 1858
- Qin Y, Lou S, Shi P, Qi Q, Zeng W, Scott PJ et al (2024) Optimisation of process parameters for improving surface quality in laser powder bed fusion. Int J Adv Manuf Technol 130:2833–2845
- Narasimharaju SR, Liu W, Zeng W, See TL, Scott P, Jiang X et al (2021) Surface texture characterization of metal selective laser melted part with varying surface inclinations. J Tribol 143(5):051106
- 31. Sohal A, Kumar K, Kumar R (2022) Heat transfer enhancement with channel surface roughness: a comprehensive review. Proc Inst Mech Eng C J Mech Eng Sci 236(11):6308–6334

- Townsend A, Pagani L, Scott PJ, Blunt L (2019) Introduction of a surface characterization parameter Sdr prime for analysis of reentrant features. J Nondestr Eval 38:58
- 33. Kuner MC, Romedenne M, Fernandez-Zelaia P, Dryepondt S (2020) Quantitatively accounting for the effects of surface topography on the oxidation kinetics of additive manufactured Hastelloy X processed by electron beam melting. Addit Manuf 36:101431
- Wu Z, Narra SP, Rollett A (2020) Exploring the fabrication limits of thin-wall structures in a laser powder bed fusion process. Int J Adv Manuf Technol 110:191–207
- 35. Holland JH (1973) Genetic algorithms and the optimal allocation of trials. SIAM J Comput 2(2):88–105
- Tipping ME (2001) Sparse Bayesian learning and the relevance vector machine. J Mach Learn Res 1:211–244
- Fisher RA (1966) The design of experiments (Eighth edn). Oliver and Boyd Edinburgh
- Mandloi K, Allen A, Cherukuri H, Miller J, Duttrer B, Raquet J (2023) CFD and experimental investigation of AM surfaces with different build orientations. Surf Topogr Metrol Prop 11(3):034001
- Coathup MJ, Blunn GW, Flynn N, Williams C, Thomas NP (2001)
   A comparison of bone remodelling around hydroxyapatite-coated, porous-coated and grit-blasted hip replacements retrieved at postmortem. J Bone Joint Surg Br Vol 83(1):118–123
- 40. Bai R, Liang G, Cheng H, Naceur H, Coutellier D, Zhao J et al (2023) Optimizing additive manufacturing path pattern for Ti-6Al-4V thin rods using a combinatorial radial basis function surrogateassisted genetic algorithm. Mater Des 236:112447

**Publisher's Note** Springer Nature remains neutral with regard to jurisdictional claims in published maps and institutional affiliations.

